# An Ultra-thin Printable Nanocomposite Sensor Network for Structural Health Monitoring

Yaozhong Liao[†§a], Pengyu Zhou[†§a][a], Dongyue Pan[a], Li-min Zhou[a] and Zhongqing Su[*a,b]

[a] Department of Mechanical Engineering

The Hong Kong Polytechnic University, Kowloon, Hong Kong SAR

[b] The Hong Kong Polytechnic University Shenzhen Research Institute

Shenzhen 518057, PR China

**Submitted to *Structural Health Monitoring-An International Journal***

**(APWSHM-2018 Special Issue)**

(initially submitted on 2nd April 2019; revised and resubmitted on 24th May 2019)

[†] PhD Student.

[§] These authors contributed equally to the work.

[*] To whom correspondence should be addressed. Tel.: +852-2766-7818, Fax: +852-2365-4703; Email: Zhongqing.Su@polyu.edu.hk (Prof. Zhongqing SU, *Ph.D.*)

**Abstract**

A nanocomposite-based sensor ink made from carbon black (CB) and polyvinyl pyrrolidone (PVP) was developed for fabricating a new breed of sensor by an inkjet printing approach, to accommodate the general purposes of structural health monitoring (SHM). This ink can be directly deposited onto the surface of various substrates or engineering structures such as polyimide film via computer-aided design to configure nanocomposite sensor arrays or dense sensor networks. Strong structure adaptability and high flexibility make this sensor a promising candidate to alternate traditional piezoresistive and piezoelectric sensors, in signal acquisition of dynamic disturbance on complex engineering structures. Lightweight and without the need to use wires or cables, the printed sensor network significantly reduces the weight and volume penalty imposed on the host structures, even when the network is deployed at a large scale. It also minimizes the possibility of exfoliation of the sensors from the host structure under cyclic load. The printed pattern distinguishes superior performance in the perception of acousto-ultrasonic signals from static up to 500 kHz, with high signal-to-noise ratio, sensitivity, and fidelity. By virtue of the tunneling current between two adjacent nanoparticles that are in close proximity (within several nanometers), the printed sensor network is capable of perceiving ultrasonic waves. The fabrication process of the sensor network does not entail any specially made printing facilities, and the CB/PVP hybrid can easily be injected into an inkjet cartridge for printing. Several confirmatory experiments and a proof-of-concept test were carried out based on the printed sensor network to validate the capability of the printed sensor for SHM.

***Keywords*:** printable sensor network; nanocomposite ink; ultra-thin film sensor; damage localization; ultrasonic waves; structural health monitoring

## 1. Introduction

Engineering structures operating in harsh environments or under heavy loads are prone to develop corrosion or fatigue damage, resulting in irremediable disasters.[1] Early detection of undersized damage in the scale of several millimeters has been facilitated by numerous damage detection methods developed in recent decades, typified as eddy current nondestructive testing, laser interferometry measurement, and ultrasonics based structural health monitoring (SHM), to name a few.[2-6] Among these approaches, ultrasonics based SHM has been widely utilized to implement real-time monitoring of the operation and health status of engineering assets, using various piezoelectric sensors such as piezoelectric lead zirconate titanate (PZT) and transducers that can be utilized to perceive guided ultrasonic waves (GUWs). However, certain drawbacks of these piezoelectric sensors have limited the further development of SHM. For instance, because the PZT wafer, like most ceramics, has low ductility and poor flexibility, it cannot be externally mounted onto surfaces with arbitrary surfaces. Moreover, the possible exfoliation of such sensors from host structures under cyclic loads or chemical corrosion makes their use debatable in high-end applications such as SHM for aircraft. To meet the strict requirements of engineering industries, diverse nanoparticle based composites have been investigated in light of rapidly developing nanotechnology and the discovery of new types of nanofiller.[7-9] These nanofiller candidates can be well dispersed in polymers to form a conductive sensing network within the matrix while a properly selected polymer matrix makes it more compatible with the host structure.

In recent years, much effort has been directed to the development of novel nanocomposite sensors for capturing signals induced by vibrations, temperature variations, and so on.[10-15] Cheng et al. demonstrated a stretchable and highly sensitive graphene based sensor that could be used to detect large deformations and monitor human motions.[10] In that study, a

"compression spring" structure was designed to significantly increase the stretchability of the bending sensor, which made it more suitable for large deformation. Casiraghi et al. designed a printable nanocomposite sensor array on paper for capturing low frequency vibrations with a gauge factor up to 150.[11] The sensing properties of this heterostructure based strain gauge were optimized by controlling printing parameters such as drop-spacing and number of print passes. Although those flexible sensors could respond to large strain with high sensitivity, it was still difficult for them to respond with GUWs that feature ultrahigh frequency beyond hundreds of kHz and ultralow magnitude at microstrain or even nanostrain scale.

Recent developments in quantum science have encouraged many researchers to develop innovative sensors with intelligent use of tunneling current, significantly increasing the sensitivity of nanocomposites in perceiving ultraweak disturbances induced by GUWs.[16-19] Hu et al. set up a numerical model to demonstrate that the sensitivity of nanocomposites could be increased by exploiting the tunneling effect.[18] The theory was verified by a polymer/CNT nanocomposite possessing a higher gauge factor than traditional strain gauge sensors under a low strain range, pointing out a nonlinear increase in resistance change. The tunneling effect, on which basis electrons can still jump from one nanoparticle to a neighboring one when they are in close proximity within several nanometers, has been widely considered the dominant sensing mechanism that can increase the sensitivity and sensing frequency range of nanofiller based composite sensors under microstrain. Making use of a tunneling effect based sensing mechanism, the sensor flakes made of carbon nanofillers and polyvinylidene fluoride (PVDF) reported in our previous work featuring enhanced electrical, mechanical and sensing properties compared with conventional piezoresistive and piezoelectric sensors.[20-22]

To minimize the dependence of sensor installations on the use of adhesives and wires, we earlier developed a sprayable sensor that could be sprayed directly onto a structural surface and respond to signals across a broadband frequency range. Problems remained, however, the thickness and density of the sensor films could be influenced by human operation errors, for example in the force and spraying time applied in each sensor fabrication process. In the present study, a nanocomposite sensor membrane, fabricated by carbon black and polyvinyl pyrrolidone (denoted hereinafter by CB/PVP), was developed by using an inkjet printing technology to precisely design and control the shapes and qualities of nanocomposite sensors. The mechanical and chemical properties of the nanocomposite sensor have been investigated elsewhere.[21, 22] The sensing abilities of this printable sensor were verified via several confirmatory experiments in the laboratory, from quasi-static vibrations to GUWs. On the basis of the experimental results, a proof-of-concept application was implemented to localize the impact damage on a carbon fiber epoxy plate of an aircraft structure, indicating that this novel sensor could be further used in some SHM applications.

## 2. Development of Printable Sensor Networks

### 2.1 Nanocomposite Ink Preparation

PVP powder with a molecular weight of 40,000 (PVP K-30, acquired from DASHAN BIO Corporation, China) was chosen as the matrix of the nanocomposite sensor, because it could be easily dissolved in both aqueous and organic solvents, forming a homogeneous solution with suitable viscosity, which is one of the essential parameters for printing.[23, 24] CB with an average diameter of 50 nm (BP2000, supplied by CABOT Corporation, USA) was chosen as the nanofiller to prevent clogging of the nozzle (supplied by Fujifilm, USA), for which the aperture is 21 μm. 1-Methyl-2-pyrrolidinone (NMP) (with a boiling point of 203 °C, supplied by J&K Scientific, China), which is hard to volatilize, was chosen as the solvent in

case of premature volatilization that can lead to resin curing inside the nozzle. The CB nanoparticles, together with PVP powder (mass ratio 1:2), were dispersed into NMP solvent, with a weight ratio of 5 wt%. Then the mixture was mechanically stirred for 2 hours at the speed of 400 rpm for homogenization. After that, the mixed ink was dispersed in an ultrasonic bath for 30 mins with the power of 50%. 300-nanoscale filter paper was used to filter large aggregations of the hybrid.

### 2.2 Sensor Fabrication and Morphological Characteristics

The ink was loaded in an inkjet cartridge (Dimatix Materials Cartridge DMC-11610, USA) with a volume of 10 pL. The printouts were deposited on various substrates by a desktop inkjet printer (PiXDRO LP50, supplied by OTB Solar - Roth & Rau, the Netherlands) upon a heated platform with a maximum heating temperature of 50 °C.

Six nanocomposite sensors, deposited on a glass fiber epoxy plate (measuring 280 mm × 200 mm × 1 mm) with a designed rectangular geometry of 20 mm × 10 mm, were gradually cured under 50 °C on the heated platform layer by layer to configure a sensor network, as presented in Figure 1(a). It is noteworthy that the shape of this printed sensor could be designed variously to fit different types of engineering structures with complex surfaces. The printed sensor shows good stability in signal acquisition, partially attributable to the good adhesion between the printed sensor and the substrates. Such good adhesion minimizes the probability of sensor exfoliation from the host structures in harsh working environments.

Polyimide (PI) film is widely used as an insulating film because of its high thermal stability, good chemical resistance, and excellent mechanical properties.[25] To achieve a good adhesion and uniform surface, the film was pre-treated by a plasma cleaner (PDC-002, Harrick

Plasma, USA) to conduct a deoxidation treatment that can increase the surface energy of the film, resulting in a lower contact angle of the ink, whereby a good adhesion between the ink and the substrate can be achieved.[26] The nanocomposite ink deposited on the PI film can be easily tailored into individual sensors. Simultaneously, the PI film can act as an insulating layer when the sensor was mounted on a conductive surface, preventing short circuiting between sensors. This present sensor, with good resilience and flexibility, can be easily manipulated to adapt to a wide variety of structures, as depicted in Figure 1(b).

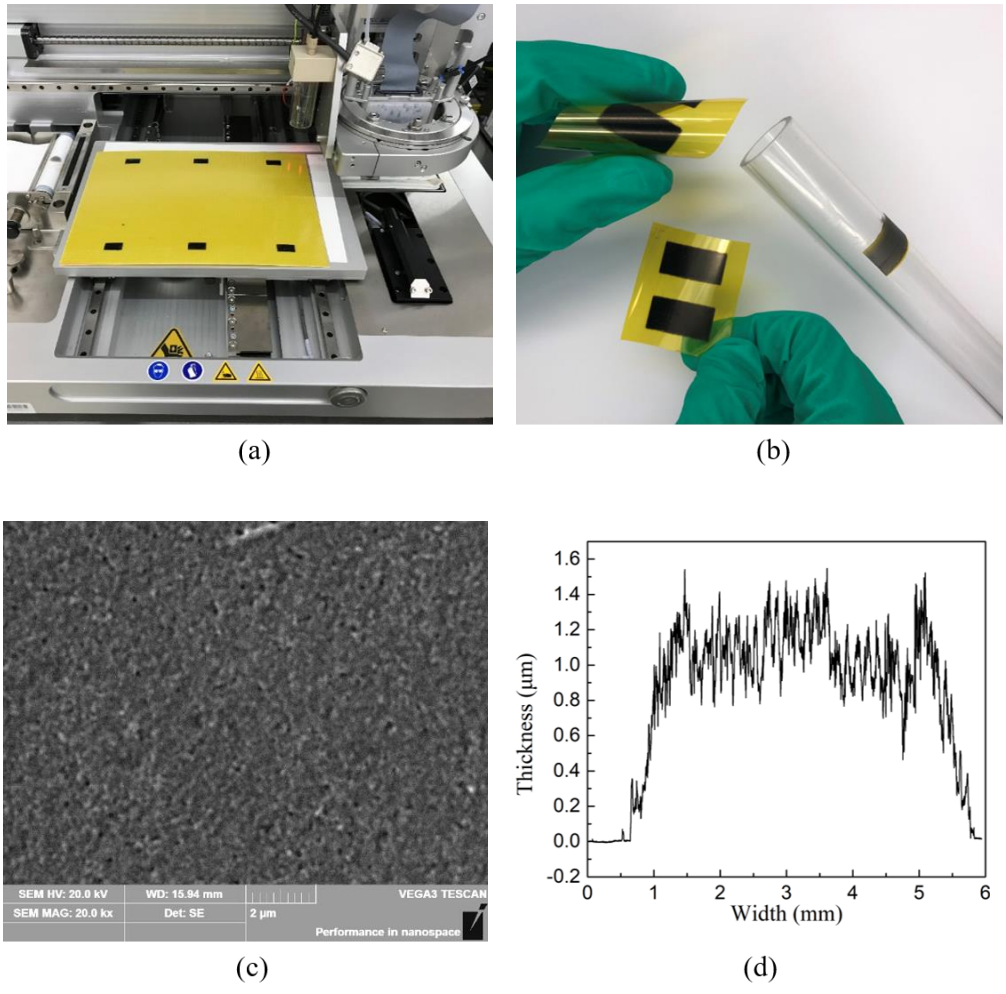


(a) (b)

(c) (d)

**Figure 1.** (a) Nanocomposite sensors printed on a glass fiber epoxy plate; (b) Nanocomposite sensors printed on PI film; (c) SEM image of the printed sensor's surface; (d) The thickness of the printed sensor along the width direction.

The surface condition of the nanocomposite was investigated by a scanning electron microscope (SEM, Vega3, supplied by Tescan, Czechoslovakia). As shown in Figure 1(c), the morphology of the printed sensor is observed compact and uniform, owing to the high resolution of the desktop printer with 16 nozzles supplying the ink simultaneously. Due to the tiny scale of CB, uniform dispersion of CB may not be observed in the SEM image explicitly, however aggregation of CB is not noted.

The thickness of the printed sensor was measured by a surface optical profiler (Dektak XT, supplied by Bruker, USA). An ultra-thin nanocomposite sensor with the thickness of ~1000 nm is observed in Figure 1(d). As observed, slight fluctuation in sensor thickness exists, however such fluctuation would not downgrade the accuracy of measurement – that is because the sensing mechanism of the sensor is the tunnelling effect which is triggered among conductive nanofillers at the nanoscale when the dynamic strain applied on the sensor. At the nanoscale, the tunneling effect would not be affected by the macroscopic discrepancy in the sensor thickness.

### 2.3 Electro-mechanical Characteristics

A uniaxial tensile test, operated on an MTS tensile machine (Alliance RT/50, Frank Bacon, USA), was conducted to preliminarily investigate the sensitivity of the nanocomposite sensor in a quasi-static situation, while the sensor was deposited on a dogbone shaped tensile specimen, a 2 mm thick epoxy plate. In this test, a metal foil strain gauge with a gauge factor of 2 was used as the reference sample to quantitatively calibrate the gauge factor of our nanocomposite sensor. A two-probe resistance measurement method was used to measure the change in resistance of the printed sensors via a dynamic digital multimeter (Keithley DMM7510, USA). As can be observed from Figure 2, the printed nanocomposite sensor

possesses a higher gauge factor (k = ~6.4), indicating higher sensitivity than that of a traditional strain gauge (k = 2), demonstrating a promising application for SHM. It can also be found that the fitting curve of the signal acquired by the printed sensor consisted of a linear fitting curve and a nonlinear fitting curve. The linear change of resistivity was caused by the piezoresistive effect when the sensor was subjected to a large deformation. In the low strain range, a quadratic and an even higher order fitting curve resulted in a higher coefficient of determination (R-squared). This phenomenon was predominantly caused by distance variations between CB nanoparticle aggregations at nanometer scale due to the tunneling effect.

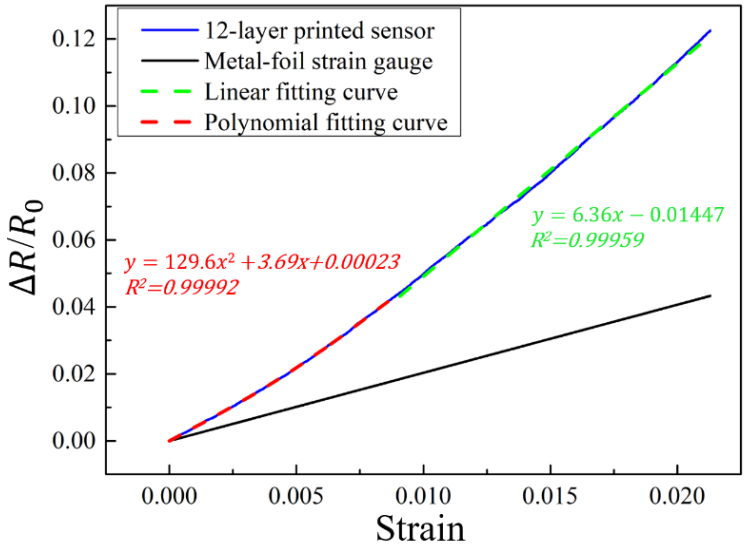


**Figure 2.** Resistance change ratio of the printed sensor under quasi-static tensile testing.

## 3. Results and Discussion

Following the preparation of the nanocomposite sensor, its sensing performance was evaluated by several experiments. Patterns were directly deposited on the surface of glass fiber epoxy plates. A 4-channel oscilloscope (Agilent® DSO9064A, Keysight Technologies, USA) with an analog bandwidth of 600 MHz was employed to collect signals simultaneously

and all channels were synchronized to ensure the consistency of data collection. A low frequency waveform generator (7075, Hioki, Japan) and a PXI (PCI extensions for instrumentation) bus platform (PXIe-1071, National Instruments, USA) were used to excite low frequency vibration and GUWs, respectively.

### 3.1 Acquisition of Structural Vibration Signals

A cantilevered beam (280 mm in length, 30 mm in width and 1 mm in thickness), trimmed from the glass fiber epoxy plate prepared in section 2, was adhered to a force transducer (8200, B&K®, Denmark) installed on an electro-mechanical shaker (4809, B&K®, Denmark) for low frequency vibration testing, as presented in Figure 3(a). A sinusoidal signal generated by the low frequency waveform generator was transmitted to the beam under different frequencies through the adhesion point 200 mm from the clamped end via the shaker. Good consistency and reversibility of the vibration signal can be observed at each cycle of the response signals acquired by the nanocomposite sensor in the low frequency range from 200 to 1000 Hz with slight fluctuations, as indicated in Figure 3(b). The response signals, acquired by the nanocomposite sensor and by a metal foil strain gauge that was adhered to the back of the beam, show good consistency without any obvious hysteresis, upon processed with a fast-Fourier-transformation-based filter, as shown in Figure 3(c). A half-cycle delay is noted, which is owing to the fact that the two types of sensors were placed at the front and back surfaces of the beam, respectively. From Figure 3(d), the intensity of the signal increases proportionally with the rise in excitation voltage, a result validating the applicability of the response signal for quantitatively reflecting the strain values.

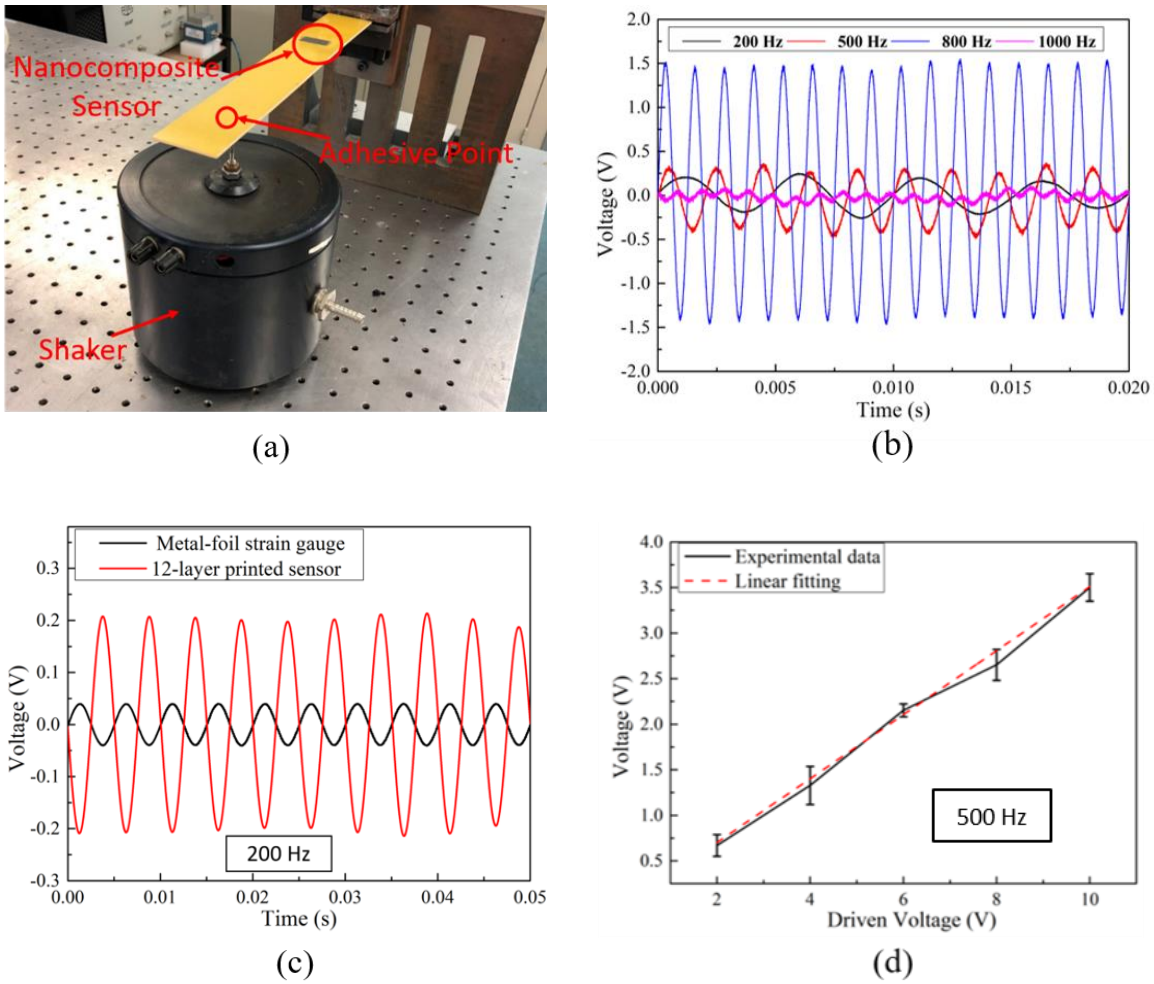


**Figure 3.** (a) Photograph of experimental setup for low frequency vibration acquisition; (b) Electro-mechanical responses of the printed sensor to vibration at representative frequencies from 200 Hz to 1000 Hz; (c) Response of the printed sensor at 200 Hz compared with metal foil strain sensor; (d) Relationship between response of the printed sensor against driven voltage at 500 Hz.

### 3.2 Acquisition of Acoustic Emission Signals

A nanocomposite sensor was randomly chosen from the sensor network to detect the medium-frequency acoustic emission (AE) signals induced by a ball drop. As illustrated in Figure 4, the impact spot was set 15 cm from the printed sensor and a PZT wafer (Physik

Instrumente Co. Ltd., PIC151; diameter: 9 mm; thickness: 0.5 mm) was surface-mounted on the glass fiber epoxy plate as a comparison sensor.

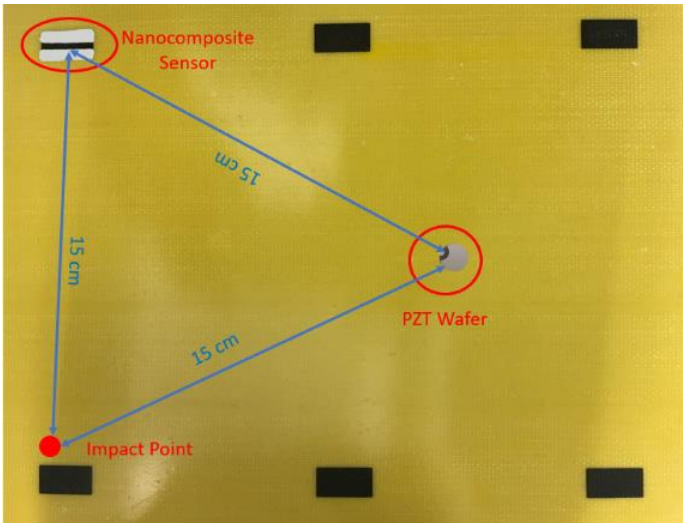


**Figure 4.** Schematic of experimental setup for AE signal acquisition.

A steel ball was freely dropped from a height of 30 cm to strike the plate and the impact signals were captured by the two sensors, as presented in Figure 5(a). The impact signal was successfully captured by the printed sensor with acceptable intensity and an unambiguous waveform, featuring good coincidence with that acquired by the PZT wafer without obvious delay in the arrival time of wave packets in the early stage. Note that there exists a certain degree of discrepancy after the first-arrival wave pack in signals captured by the nanocomposite sensor and the PZT wafer, which can be attributed to the different locations of the nanocomposite sensor and the PZT wafer, and the scattered waves from the boundary lead to such discrepancy. Here, we present a proof-of-concept experiment to validate the capability of the developed nanocomposite sensors in perceiving the first-arrival signal, by using the commercial PZT wafers as a reference. In the validation, the arrival time and waveform of the first-arrival wave pack are of the key interest. Then the acquired signal was filtered by a fast-Fourier-transformation based algorithm with a cutoff frequency of 10 kHz.

No sensible difference could be observed between the original and filtered signals, a result that highlights the stable sensing ability of the nanocomposite sensor, as depicted in Figure 5(b).

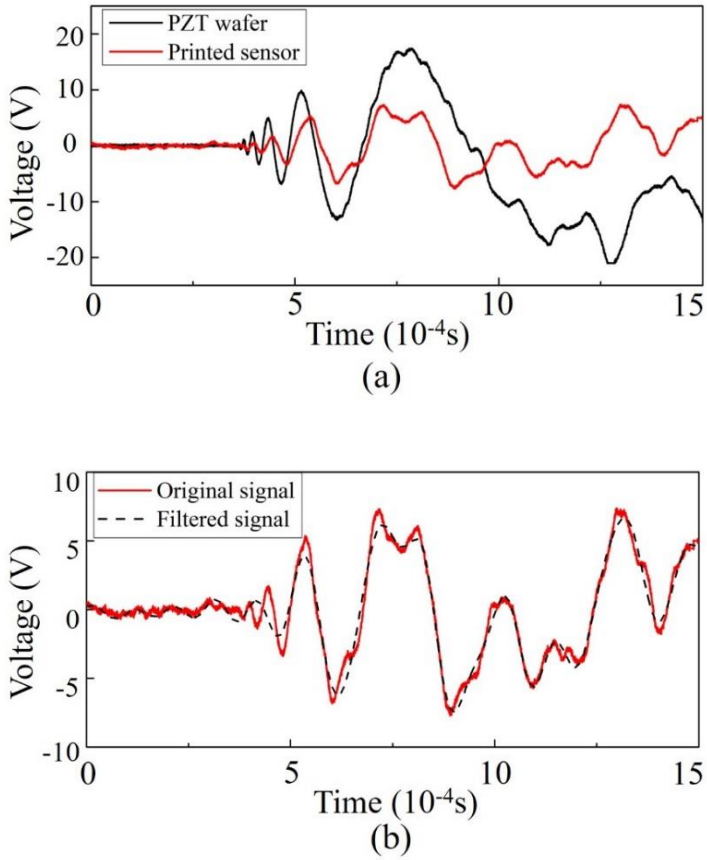


**Figure 5.** (a) Impact signals acquired using two sensors; (b) Comparison of impact signals acquired by the printed sensor with/without noise filtering.

### 3.3 Acquisition of Guided Ultrasonic Waves

Because the magnitude of the strain induced by GUWs is extremely low, the appropriately generated resistivity variation of the printed sensor may be easily obscured by ambient noise. To further investigate the sensing ability of this sensor in the ultrahigh frequency regime, a self-developed Wheatstone bridge with cutoff frequencies between 100 Hz and 1500 kHz

was designed to amplify the signal by transferring the resistivity change into a voltage change with 1000 times amplification. Two PZT wafers were used as actuator and counterpart sensor, respectively.

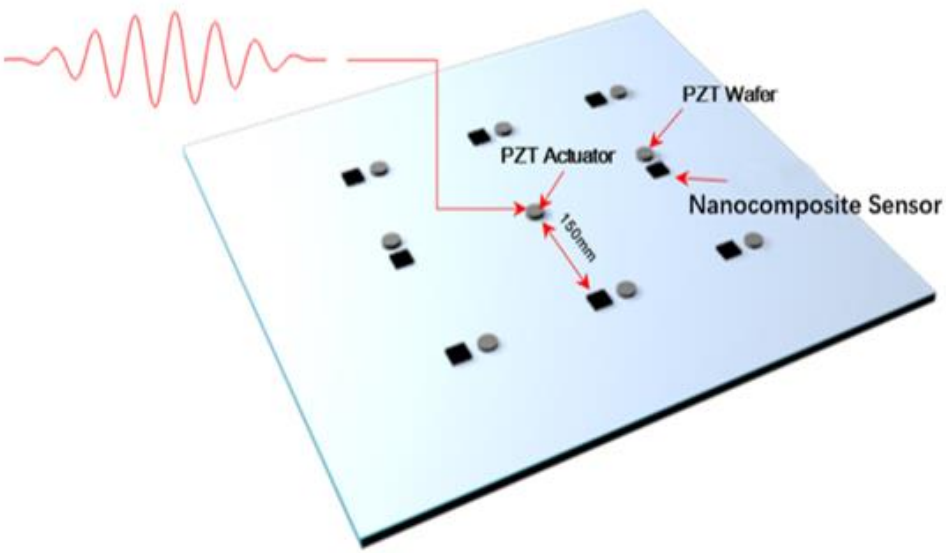


**Figure 6.** Schematic of experimental setup for GUWs acquisition.

A PZT wafer was used to generate GUWs 15 cm from the nanocomposite sensor, as shown in Figure 6. As can be observed from Figure 7(a), a five-cycle Hanning-windowed sinusoidal tone burst signal, excited by the actuator at a central frequency of 175 kHz with an excitation voltage of 1 V after being amplified 200 times by a linear power amplifier (Ciprian® US-TXP-3, French), was received by the nanocomposite sensor with high signal-to-noise ratio (SNR) and high fidelity. There is no obvious discrepancy between the first arriving wave packet (zeroth order symmetric Lamb wave mode ($S_0$)) acquired by both printed sensor and PZT wafer in both waveform and arrival time, even though they have different sensing mechanisms – a piezoresistive effect for the nanocomposite sensor and a piezoelectric effect for the PZT wafer. The sensing frequency limitation of the nanocomposite sensor was investigated by gradually increasing the excitation frequency from 50 kHz to 500 kHz. By

285 virtue of the weak excitation intensity, a significant decrease in the signal magnitude can be
286 observed from the signal at 500 kHz (processed by a low pass filter with a cutoff frequency
287 of 350 kHz and 650 kHz because the signal was severely masked by environmental noise),
288 as shown in Figure 7(b). The crosstalk, which occurred at initiation, was induced mainly by
289 circuit disturbance.
290

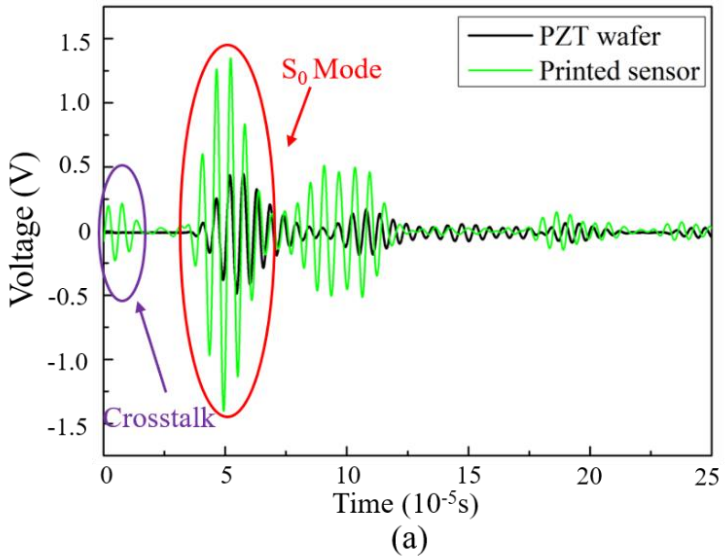


291

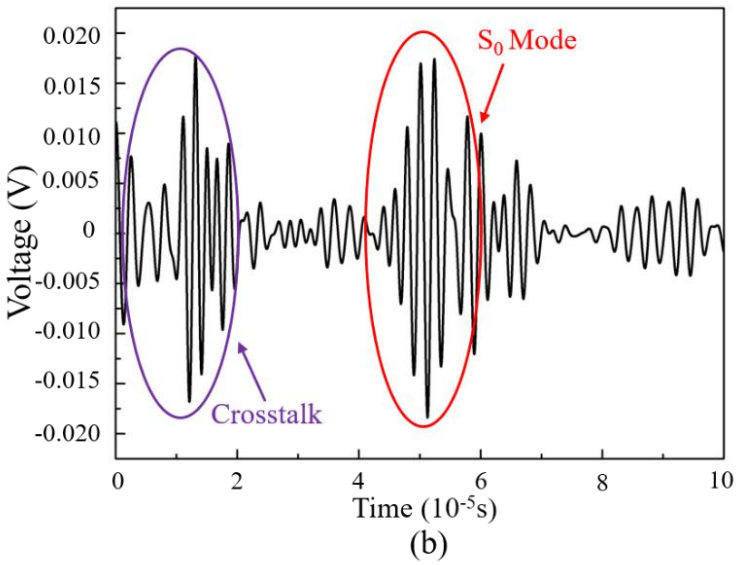


292

293 **Figure 7.** GUWs signal acquired at: (a) 175 kHz using both printed sensor and PZT wafer;
294 (b) 500 kHz using printed sensor.
295

296 As illustrated in Figure 8, the magnitude of the acquired signal was extracted from the data
297 at 200 kHz and was used for clear observation of the trend between the signal amplitude
298 acquired by three types of nanocomposite sensor against the driven voltage. The result
299 proves that this CB based printed sensor is able to quantitatively reflect the intensity of
300 variation of the host engineering structure in such high-frequency regime. Compared with
301 the signals acquired by the nanocomposite sensors fabricated in our previous work, it is
302 found that: (1) the CB based printed sensor sheds light on much higher sensitivity than the
303 CB based hot-pressing sensor; (2) the CB based printed sensor has the highest accuracy and
304 the lowest sensing errors among three nanocomposite sensor types, although the graphene
305 based hot-pressing sensor has the highest sensitivity. Owing to the precise fabrication
306 process of the inkjet printing technology, this printed sensor can function stably with
307 accurate performance.
308

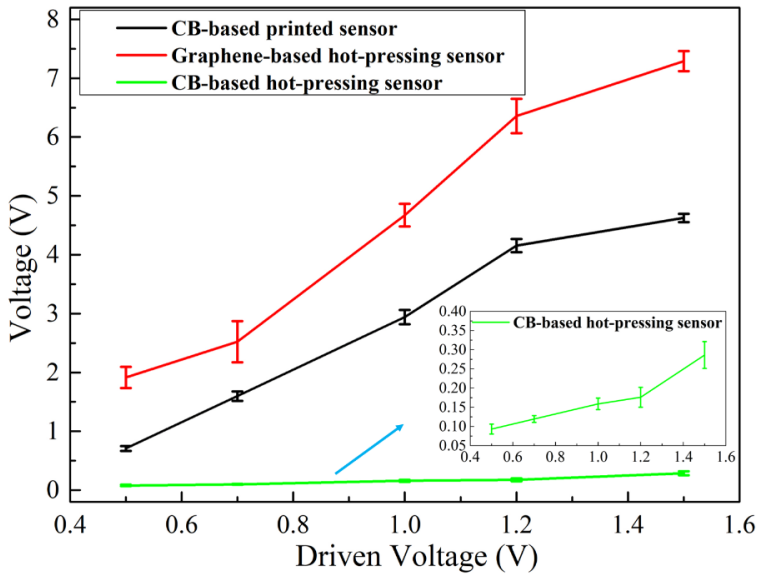

309

310 **Figure 8.** Signal amplitude of acquired GUWs under different driven voltages at 200 kHz.

## 4. Proof-of-concept Application: Impact Damage Localization Using Printed Sensor Network

In view of the high quality of the characteristics of the acquired signal, a proof-of-concept test was conducted. Four sensor films were mounted on a carbon fiber plate 20 cm from the center in a cruciform shape, as shown in Figure 9. The impact energy and impact point could be quantitatively evaluated, based on the signal acquired by the printed sensors, using the delay-and-sum algorithm.[27]

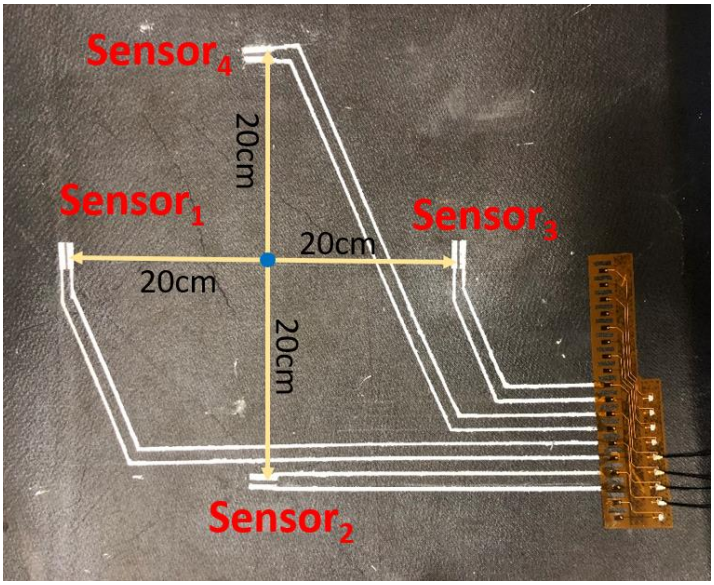


**Figure 9.** Photographic diagram of the printed sensor network on a carbon fiber epoxy plate.

Passive localization of impact damage was implemented using a percussion hammer to impact the carbon fiber plate of an aircraft structure. A painted circuit was introduced to link the sensor network to a flexible circuit board to which four knock-down electrical wires were connected. The AE signals were perceived sequentially by those sensors, depending on their distance from the impact point, as illustrated in Figure 10. Because the raw data of the acquired signals was unambiguous with a high SNR, the arrival time and impact intensity

could be identified clearly to further quantitatively evaluate the severity and location of the impact damage. With the known location of the four sensors ($x_i$, $y_i$), the travelling time $\Delta t_i$ for the low velocity impact induced zeroth order antisymmetric mode signal (denoted by $A_0$) between two individual sensors *i* and *j* (denoted by $S_i$ and $S_j$) could be expressed as:

$$\Delta t_{ij} = t_j - t_i \tag{1}$$

where $t_i$ and $t_j$ represent the travelling time of the $A_0$ wave from the impact point to the printed sensors. Now, taking the four sensors ($S_1$, $S_2$, $S_3$, $S_4$) into consideration while using $S_1$ as the reference sensor, the distance between $S_i$ and impact point P$(a, b)$ could be calculated as:

$$\begin{cases} (a-x_1)^2 + (b-y_1)^2 = v^2 {t_1}^2 \\ (a-x_2)^2 + (b-y_2)^2 = v^2 {t_2}^2 = v^2 (t_1 + \Delta t_{12})^2 \\ (a-x_3)^2 + (b-y_3)^2 = v^2 {t_3}^2 = v^2 (t_1 + \Delta t_{13})^2 \\ (a-x_4)^2 + (b-y_4)^2 = v^2 {t_4}^2 = v^2 (t_1 + \Delta t_{14})^2 \end{cases} \tag{2}$$

where $v$ is the velocity of the $A_0$ wave in the carbon fiber epoxy plate. The impinged spot can be calculated via Equation 2 with the known location of the four sensors and the time delay $\Delta t_{ij}$. Based on these characteristics extracted from the raw data, the impact severity could be structured by a two-dimensional grayscale image via its pixel value ($\delta_{ij}(x, y)$):

$$\delta_{ij}(x, y) = \max\left(E_i + E_j\left(\Delta t_{ij}(x, y)\right)\right) \tag{3}$$

where $E_i$ is the energy of the $A_0$ mode using a wavelet transform. The impact severity could be referred to the summation of peak energy acquired by the four sensors with compensation for the time delay $\Delta t_{ij}(x, y)$.

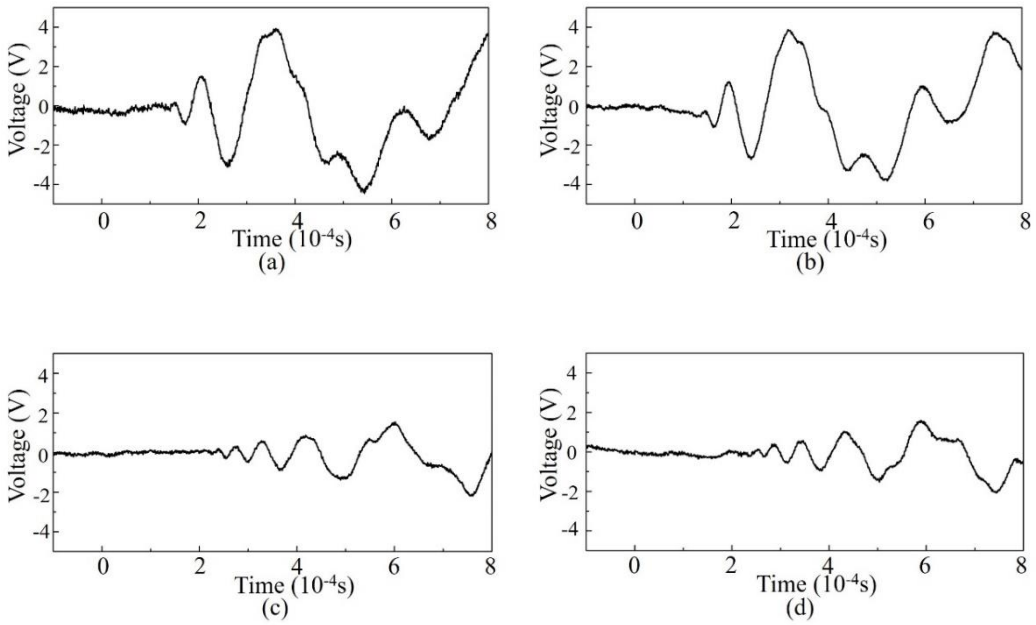


**Figure 10.** Impact signal acquired by: (a) $Sensor_1$; (b) $Sensor_2$; (c) $Sensor_3$; (d) $Sensor_4$.

From the results in Figure 11, an accurate point of impact and severity of the damage were localized and evaluated with acceptable error using only four sensors. Subsequently, a higher pixel value can indicate a higher probability of the point of impact.

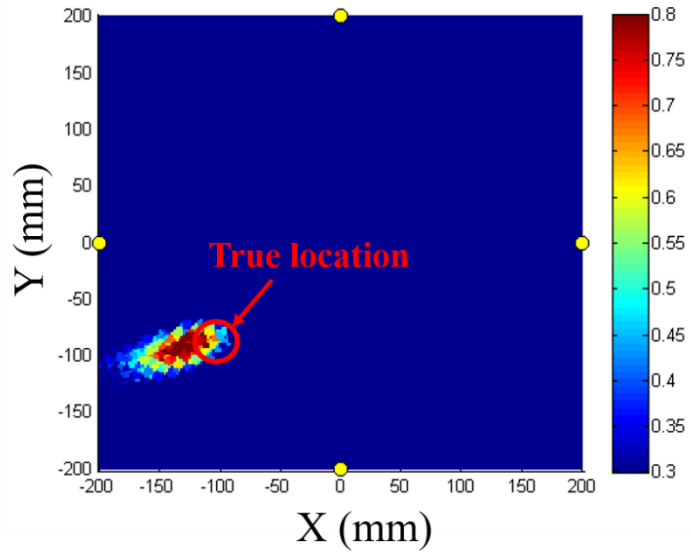


**Figure 11.** Comparison between identified and real point of impact using AE signals captured by the printed sensors.

## 5. Concluding Remarks

A printable sensor that can be deposited directly onto the surface of an engineering structure was fabricated to capture vibration signals. Without the use of an adhesive compound, this innovative sensor is capable of being tightly integrated with the host structure. Meanwhile, this fabricated sensor introduces no significant weight or volume penalty to the host structure, by virtue of the low-density material used in the manufacturing process and the negligible thickness produced by the inkjet printing technology. The sensing ability of this sensor was successfully verified experimentally from quasi-static up to 500 kHz. An impact damage localization test was conducted to accurately predict the point of impact with reasonable error, revealing the excellent potential of the nanocomposite sensor for structural health monitoring.

## Declaration of Conflicting Interests

The author(s) declared no potential conflicts of interest with respect to the research, authorship, and/or publication of this article.

## Acknowledgement

This project was supported by the Hong Kong Research Grants Council via General Research Funds (Nos. 15201416 and 15212417). The work was also supported by the National Natural Science Foundation of China via a General Project (No. 51875492).

## References


1. David OO, Sullivan G, Dickens T, et al. Development of a triboluminescence-based sensor system for concrete structures. *Struct Health Monit* 2018; 11(2): 139–147.
2. Hamia R, Cordier C and Dolabdjian C. Eddy-current non-destructive testing system for the determination of crack orientation. *NDT&E Int* 2014; 61: 24-28.
3. Png WH, Lin HS, Pua CH, et al. Feasibility use of in-line Mach–Zehnder interferometer optical fibre sensor in lightweight foamed concrete structural beam on curvature sensing and crack monitoring. *Struct Health Monit* 2018; 17(5) 1277-1288.
4. Su Z, Ye L and Lu Y. Guided Lamb waves for identification of damage in composite structures: A review. *J Sound Vib* 2006; 295: 753-780.
5. Qiu L, Liu M, Qing X, et al. A quantitative multi-damage monitoring method for large-scale complex composite. *Struct Health Monit* 2013; 12(3): 183-196.
6. Janapati V, Kopsaftopoulos F, Li F, et al. Damage detection sensitivity characterization of acousto-ultrasound-based structural health monitoring techniques. *Struct Health Monit* 2016; 15(2): 143–161.
7. Hwang SH, Park HW, Park YB, et al. Electromechanical strain sensing using polycarbonate-impregnated carbon nanotube-graphene nanoplatelet hybrid composite sheets. *Compos Sci Technol* 2013; 89: 1-9.
8. Iijima S. Helical microtubules of graphitic carbon. *Nature* 1991; 354: 56-58.
9. Geim AK and Novoselov KS. The rise of graphene. *Nat Mater* 2007; 6: 183-191.
10. Cheng Y, Wang R, Sun J, et al. A Stretchable and Highly Sensitive Graphene-Based Fiber for Sensing Tensile Strain, Bending, and Torsion. *Adv Mater* 2015; 27: 7365-7371.
11. Casiraghi C, Macucci M, Parvez K, et al. Inkjet printed 2D-crystal based strain gauges on paper. *Carbon* 2018; 129: 462-467.

12. Kang D, Pikhitsa PV, Choi YW, et al. Ultrasensitive mechanical crack-based sensor inspired by the spider sensory system. *Nature* 2014; 516: 222-226.
13. Boland CS, Khan U, Backes C, et al. Sensitive, high-strain, high-rate bodily motion sensors based on graphene rubber composites. *ACS Nano* 2014; 8(9): 8819-8830.
14. Qiu L, Coskun BM, Tang Y, et al. Ultrafast dynamic piezoresistive response of graphene-based cellular elastomers. *Adv Mater* 2016; 28(1): 194-200.
15. Liu S, Wu X, Zhang D, et al., Ultrafast dynamic pressure sensors based on graphene hybrid structure. *ACS Appl Mater Interfaces* 2017; 9(28): 24148-24154.
16. Amjadi M, Kyung KU, Park I, et al. Stretchable, skin-mountable, and wearable strain sensors and their potential applications: a review. *Adv Funct Mater* 2016; 26(11): 1678-1698.
17. Hu N, Itoi T, Akagi T, et al. Ultrasensitive strain sensors made from metal-coated carbon nanofiller/epoxy composites. *Carbon* 2013; 51: 202-212.
18. Hu N, Karube Y, Yan C, et al. Tunneling effect in a polymer/carbon nanotube nanocomposite strain sensor. *Acta Mater* 2008; 56(13): 2929-2936.
19. Hu N, Karube Y, Arai M, et al. Investigation on sensitivity of a polymer/carbon nanotube composite strain sensor. *Carbon* 2010; 48(3): 680-687.
20. Zeng Z, Liu M, Xu H, et al. Ultra-broadband frequency responsive sensor based on lightweight and flexible carbon nanostructured polymeric nanocomposites. *Carbon* 2017; 121: 490-501.
21. Liao Y, Duan F, Zhang H, et al. Ultrafast response of spray-on nanocomposite piezoresistive sensors to broadband ultrasound. *Carbon* 2019; 143: 743-751.
22. Duan F, Liao Y, Zeng Z, et al. Graphene-based nanocomposite strain sensor response to ultrasonic guided waves. *Compos Sci Technol* 2019; 174: 42-49.

429 23. Derby B. Inkjet Printing of Functional and Structural Materials: Fluid Property
430 Requirements, Feature Stability, and Resolution. *Annu Rev Mater Res* 2010; 40: 395-
431 414.
432 24. Fromm JE. Numerical Calculation of the Fluid Dynamics of Drop-on-Demand Jets. *IBM*
433 *J Res Dev* 1984; 28: 322-333.
434 25. Liaw D, Wang K, Huang Y, et al. Advanced polyimide materials: Syntheses, physical
435 properties and applications. *Prog in Polym Sci* 2012; 37(7): 907-974.
436 26. Inagaki N, Tasaka S and Hibi K. Surface modification of Kapton film by plasma
437 treatments. *J Polym Sci Part A: Polym Chem* 1992; 30: 1425-1431.
438 27. Liu M, Zeng Z, Xu H, et al. Applications of a nanocomposite-inspired *in-situ* broadband
439 ultrasonic sensor to acousto-ultrasonics-based passive and active structural health
440 monitoring. *Ultrasonics* 2017; 78: 166-174.